

# Fluctuation-induced transport in the Hall plasma accelerator

Cliff A. Thomas\*, and Mark A. Cappelli†

*Stanford University, Stanford, CA, 94305-3032, United States*

This paper considers small-amplitude fluctuations in the Hall-effect thruster. To predict which fluctuations could be important to transport, the growth of a disturbance is determined as a function of real frequency and propagation angle. In the simple case, strong growth is predicted for disturbances that are azimuthal. In the general case, strong growth is predicted for various propagation angles. To determine if these modes could explain the mobility, the phase separating fluctuations in the velocity and number density is estimated. Significant transport is predicted for disturbances in certain frequency/wavenumber regimes. As a consequence, it is concluded that small-amplitude fluctuations could explain the transport in the Hall-effect thruster, and that spatial variation in the oscillation spectra could account for position dependent electron mobility.

## Nomenclature

$\Phi$	Potential (V)
$\mathbf{E}$	Electric Field (V/m)
$\mathbf{B}$	Magnetic Field (T)
$\mathbf{k}$	Wavenumber (rad/m)
$\omega$	Frequency (rad/s)
$\mu_o$	Magnetic Permeability (H/m)
$\epsilon_o$	Dielectric Constant (F/m)
$k_b$	Boltzmann Constant (J/K)
$n_\alpha$	Number Density ( $1/\text{m}^3$ )
$c_\alpha$	Thermal Velocity (m/s)
$q_\alpha$	Charge (C)
$m_\alpha$	Mass (kg)
$T_\alpha$	Temperature (K)
$P_\alpha$	Pressure (Pa)
$\nu_\alpha$	Collision Rate ( $1/\text{s}$ )
$\mathbf{U}_\alpha$	Velocity (m/s)

## I. Introduction

THE Hall plasma accelerator, or Hall-effect thruster (HET), is a coaxial discharge characterized by its orthogonal electric and magnetic field.<sup>1</sup> It uses its applied magnetic field to modify its local electron mobility, and shape its accelerating electric potential. The magnitude of  $\mathbf{B}$  is small, so ions are not magnetized, and they slide down the resulting potential hill. The plasma discharge occurs inside a coaxial acceleration channel (usually a ceramic). The propellant is typically a mono-atomic gas with a low ionization cost, a large atomic mass, and a large cross-section for electron-impact ionization. The electrons in the discharge migrate towards the anode, and migrate faster where the electron mobility is high. Where the electron mobility is low however (because the magnetic field is strong), the electrons pool and execute closed  $\mathbf{E} \times \mathbf{B}$  drift.

\*Peon, Mechanical Engineering Department, Building 520, Student Member.

†Lord, Mechanical Engineering Department, Building 520, Regular Member.

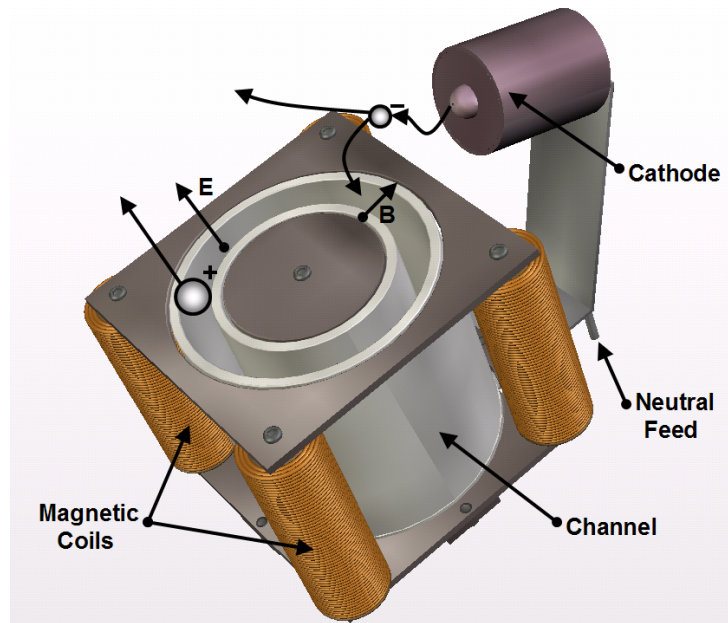


Figure 1. Diagram of a Hall-effect thruster.

Since their residence time in this region is long compared to the time period between ionizing collisions, the trapped electrons collide with neutral propellant, create more electrons, and the discharge is sustained. A hollow cathode neutralizes the space charge of the resulting ion beam (see Fig. 1).

In the typical Hall accelerator, the ions can carry 70 – 90% of the discharge current depending on the effectiveness of the design at inhibiting electron migration. Unfortunately, the rate that electrons leak through the applied magnetic field is unpredictable; this makes the magnetic field in the HET difficult to optimize. Classical diffusion theory (which scales as  $B^{-2}$ ) underestimates the cross-field transport in the HET, and numerical models of the discharge must commonly invoke an anomalous diffusion coefficient (like that of Bohm, varying as  $B^{-1}$ ) to achieve acceptable results.<sup>2</sup> An analysis by Fife<sup>3</sup> of early Russian experimental results,<sup>4</sup> and recent measurements at Stanford,<sup>5,6</sup> indicate the electron mobility (which is proportional to the inverse Hall parameter,  $(\omega\tau)^{-1}$ ) is a strong function of position. In some portions of the discharge, the measured inverse Hall parameter is close to the value given in Bohm's work,  $(\omega\tau)^{-1} = 1/16$ .<sup>7</sup> However, in those regions where the magnetic field is strongest, the mobility approaches the value expected for classical diffusion. The reason for this observation is a subject of considerable debate,<sup>8,9</sup> but anomalous transport is usually attributed to fluctuations in the potential and/or electron-wall interactions.

This paper linearizes the mass and momentum conservation equations for electrons and ions to determine the dispersion relation in the Hall plasma accelerator. To predict which instabilities could impact transport, the growth of a disturbance is determined as a function of real frequency and propagation angle. In the simple case, a dispersion relation derived by Guerrini et al<sup>10</sup> is found, and strong growth is predicted for azimuthal fluctuations. In the general case, azimuthal, axial, and mixed modes are found to exhibit strong growth. To determine if these modes could explain transport in the Hall-effect thruster, the phase separating fluctuations in the velocity and number density is then estimated. Significant transport is predicted for disturbances in certain frequency/wavenumber regimes. As a consequence, it is concluded that transport in the Hall-effect thruster could result from small-amplitude fluctuations, and that spatial dependence in the time-average mobility may be explained by a position dependent oscillation spectra.

## II. Small Amplitude Oscillations

### A. The Dispersion Relation (I)

In order to assess the impact of high-frequency fluctuations on transport in the Hall-effect thruster, it is necessary to appreciate the wavenumber ( $\mathbf{k}$ ), frequency ( $\omega$ ), and phase relationship ( $\varphi$ ), of plasma property oscillations as a function of time-average quantities like the number density ( $n_\alpha$ ), bulk velocity ( $\mathbf{U}_\alpha$ ), and the applied magnetic field ( $\mathbf{B}$ ). This information is provided by the dispersion relation, a formula derived by considering the response of charged particles to fields, collisions, and other processes, for plasma property oscillations that are small (this is defined in Sec. III).

We begin this development by considering Ampere's Law, Eq. (1), and Faraday's Law of Induction, Eq. (2). Gauss's Law for Magnetism and Electricity are given by Eq. (3) and Eq. (4), respectively.

$$\nabla \times \mathbf{B} = \mu_o \mathbf{J} + \mu_o \epsilon_o \frac{\partial \mathbf{E}}{\partial t} \quad (1)$$

$$\nabla \times \mathbf{E} = -\frac{\partial \mathbf{B}}{\partial t} \quad (2)$$

$$\nabla \cdot \mathbf{B} = 0 \quad (3)$$

$$\nabla \cdot \mathbf{E} = \frac{\rho_c}{\epsilon_o} \quad (4)$$

If Eq. (2) is substituted in Eq. (1) (after taking the partial derivative in time of Eq. (2)), Eq. (5) results, an equation that permits solutions that propagate in space and time.

$$-\nabla \times \nabla \times \mathbf{E} = -\nabla(\nabla \cdot \mathbf{E}) + \nabla^2 \mathbf{E} = c^{-2} \left( \frac{1}{\epsilon_o} \frac{\partial \mathbf{J}}{\partial t} + \frac{\partial^2 \mathbf{E}}{\partial t^2} \right) \quad (5)$$

If we assume the fluctuations in the HET are electrostatic ( $\nabla \times \mathbf{E} = 0$ ), then Eq. (6) can be solved to determine the relationship between fluctuations in the potential and fluctuations in the number density and velocity. Eq. (6) is equivalent to the Poisson equation, Eq. (4).

$$0 = \left( \frac{1}{\epsilon_o} \frac{\partial \mathbf{J}}{\partial t} + \frac{\partial^2 \mathbf{E}}{\partial t^2} \right) \quad (6)$$

To account for the effect of charged particles in Eq. (6) (through the current density  $\mathbf{J}$ ), the conservation equation for each species' mass and momentum must be considered. To be more accurate, some treatment of the electron energy equation is also needed. Before proceeding, it is necessary to detail the form of the small amplitude perturbation equations considered in this text; these are given by Eq. (7) through Eq. (9).

$$\mathbf{E} = \mathbf{E}_o + \frac{\partial \mathbf{E}_o}{\partial x} x + \tilde{\mathbf{E}} \exp(i\mathbf{k} \cdot \mathbf{r} - \omega t) \quad (7)$$

$$\mathbf{U}_\alpha = \mathbf{U}_{\alpha,o} + \frac{\partial \mathbf{U}_{\alpha,o}}{\partial x} x + \tilde{\mathbf{U}}_\alpha \exp(i\mathbf{k} \cdot \mathbf{r} - \omega t) \quad (8)$$

$$n_\alpha = n_{\alpha,o} + \frac{\partial n_{\alpha,o}}{\partial x} x + \tilde{n}_\alpha \exp(i\mathbf{k} \cdot \mathbf{r} - \omega t) \quad (9)$$

Here, the axial direction is the  $\mathbf{x}$  direction, the azimuthal direction is the  $\mathbf{y}$  direction (the  $-\mathbf{E} \times \mathbf{B}$  direction), and  $\mathbf{r}$  is a position vector in  $\mathbf{x}$  and  $\mathbf{y}$ . The radial magnetic field,  $\mathbf{B}$ , is in the  $\mathbf{z}$  direction. Quantities with the subscript naught ( $o$ ) refer to steady-state values. The only unusual addition to Eq. (7) through Eq. (9) is a steady-state gradient in the axial direction. The gradient is included to account for observations, and to determine the impact of time-average  $\mathbf{E} \times \mathbf{B}$  shear.

The number density (including  $\tilde{n}_\alpha$ ) is found by considering the species continuity equation. See Eq. (10).

$$\frac{\partial n_\alpha}{\partial t} + \nabla \cdot (n_\alpha \mathbf{U}_\alpha) = 0 \quad (10)$$

Generation terms are neglected in Eq. (10), since the frequency range of interest to anomalous transport is likely an order of magnitude greater (1-10MHz versus 100kHz). To solve for the fluctuating number density, Eq. (7) through Eq. (9) are substituted in Eq. (10), and like terms collected. The static solution, or “stationary solution”, is provided by the terms without an oscillating component, evaluated at  $\mathbf{r} = 0$ ; the static solution is given by Eq. (11).

$$\frac{\partial n_{\alpha,o}}{\partial x} \mathbf{U}_{\alpha,o,x} + \frac{\partial \mathbf{U}_{\alpha,o,x}}{\partial x} n_{\alpha,o} = 0 \quad (11)$$

If the terms with one fluctuating component are collected and evaluated at  $\mathbf{r} = 0$ , the oscillating solution is found (see Eq. (12) through Eq. (14)). Products of two or more oscillating components are assumed to be negligible (since we are only considering small amplitude waves - hence, the small amplitude model). In Eq. (12), the oscillation in the number density is defined by the oscillation in the velocity.

$$\frac{\tilde{n}_\alpha}{n_{\alpha,o}} = \frac{\mathbf{k} \cdot \tilde{\mathbf{U}}_\alpha - ik_n \tilde{\mathbf{U}}_{\alpha,x}}{\omega_\alpha} \quad (12)$$

$$\omega_\alpha = \omega - \mathbf{k} \cdot \mathbf{U}_{\alpha,o} + i \frac{\partial \mathbf{U}_{\alpha,o,x}}{\delta x} \quad (13)$$

$$k_n = \frac{\delta \ln n_\alpha}{\partial x} \quad (14)$$

The velocity (including  $\tilde{\mathbf{U}}_\alpha$ ) due to an oscillation in the potential, is found by considering the species momentum equation. See Eq. (15).

$$\frac{\partial \mathbf{U}_\alpha}{\partial t} + (\mathbf{U}_\alpha \cdot \nabla) \mathbf{U}_\alpha = \frac{q_\alpha}{m_\alpha} \left( \mathbf{E} - \frac{\nabla P_\alpha}{n_\alpha q_\alpha} + \mathbf{U}_\alpha \times \mathbf{B} \right) - \nu_\alpha \mathbf{U}_\alpha \quad (15)$$

To solve for the velocity in the same manner we used to find Eq. (12), Eq. (7) through Eq. (9) are substituted in Eq. (15), and like terms collected. The system is evaluated at  $\mathbf{r} = 0$ . To account for the pressure gradient an adiabatic energy equation is used (see Eq. (16)). This is believed to be appropriate, since energy transport due to high-frequency fluctuations is believed to be “fast” (as compared to other means of energy transfer). Using Eq. (16), a simple form for the pressure gradient is derived. See Eq. (17).

$$P_\alpha \rho_\alpha^{-\gamma} = C \quad (16)$$

$$\nabla P = m_\alpha V_{\alpha,s}^2 \nabla n_\alpha \quad (17)$$

$$V_{\alpha,s}^2 = \frac{1}{m_\alpha} \gamma_\alpha k_b T_\alpha \quad (18)$$

Here, the adiabatic sound speed is given by  $V_{\alpha,s}$ . The static solution to Eq. (15) is then given by Eq. (19) and Eq. (20).

$$\mathbf{U}_{\alpha,o,x} \frac{\partial \mathbf{U}_{\alpha,o,x}}{\partial x} = \frac{q_\alpha}{m_\alpha} \left( E_{o,x} - \frac{m_\alpha V_{\alpha,s}^2}{q_\alpha n_{\alpha,o}} \frac{\partial n_{\alpha,o}}{\partial x} + (\mathbf{U}_{\alpha,o} \times \mathbf{B})_x \right) - \nu_\alpha \mathbf{U}_{\alpha,o,x} \quad (19)$$

$$\mathbf{U}_{\alpha,o,x} \frac{\partial \mathbf{U}_{\alpha,o,y}}{\partial x} = \frac{q_\alpha}{m_\alpha} \left( E_{o,y} - \frac{m_\alpha V_{\alpha,s}^2}{q_\alpha n_{\alpha,o}} \frac{\partial n_{\alpha,o}}{\partial y} + (\mathbf{U}_{\alpha,o} \times \mathbf{B})_y \right) - \nu_\alpha \mathbf{U}_{\alpha,o,y} \quad (20)$$

The fluctuating solution to Eq. (15) is given by Eq. (21) through Eq. (24). Here, Eq. (12) is used to simplify the resulting expression. The cyclotron frequency,  $\Omega_\alpha$ , is defined as  $\frac{q_\alpha}{m_\alpha} \mathbf{B} \cdot \hat{\mathbf{z}}$ .

$$\Pi_1 \tilde{\mathbf{U}}_\alpha + \Pi_2 \tilde{\mathbf{U}}_\alpha + \Pi_3 \tilde{\mathbf{U}}_\alpha = i \frac{q_\alpha}{m_\alpha} \tilde{\mathbf{E}} \quad (21)$$

$$\Pi_1 = \begin{bmatrix} \omega_\alpha + iv_\alpha & -i\Omega_\alpha \\ i\Omega_\alpha & \omega_\alpha + iv_\alpha \end{bmatrix} \quad (22)$$

$$\Pi_2 = \begin{bmatrix} 0 & 0 \\ i \frac{\partial \mathbf{U}_{\alpha,o,y}}{\partial x} & -i \frac{\partial \mathbf{U}_{\alpha,o,x}}{\partial x} \end{bmatrix} \quad (23)$$

$$\Pi_3 = \begin{bmatrix} -\frac{V_{\alpha,s}^2}{\omega_\alpha^2} k_x k_x + i \frac{V_{\alpha,s}^2}{\omega_\alpha^2} k_x k_n & -\frac{V_{\alpha,s}^2}{\omega_\alpha^2} k_x k_y \\ -\frac{V_{\alpha,s}^2}{\omega_\alpha^2} k_y k_x + i \frac{V_{\alpha,s}^2}{\omega_\alpha^2} k_y k_n & -\frac{V_{\alpha,s}^2}{\omega_\alpha^2} k_y k_y \end{bmatrix} \quad (24)$$

At this stage, it is important to point out that for steady-state measurements of  $\mathbf{E}$  and  $\mathbf{B}$ , the electron temperature, the number density, the velocity, and the electron collision rate, Eq. (21) can be solved for a defined fluctuation in the potential (since  $\tilde{\mathbf{E}} = -\nabla\tilde{\Phi}$ ). Since  $\tilde{\mathbf{U}}_\alpha$  is known, Eq. (12) can also be solved. So, in the context of small amplitude oscillations, for a known  $\tilde{\Phi}$ , both  $\tilde{\mathbf{U}}_\alpha$  and  $\tilde{n}_\alpha$  are determined. Since this solution is difficult to present in short, a simplified set of expressions is considered in this Section. If the collision frequency, the adiabatic sound speed, and the gradient quantities are assumed to be negligible, then  $\tilde{n}_\alpha$  and  $\tilde{\mathbf{U}}_\alpha$  take a simple form (see Eq. (25) through Eq. (27)). While there is no justification to support these simplifications globally, the resulting system is accurate for different regions of the HET, and provides a qualitative understanding of  $\tilde{\mathbf{U}}_\alpha$  and  $\tilde{n}_\alpha$  as a function of  $\tilde{\Phi}$ .

$$\frac{\tilde{n}_\alpha}{n_{\alpha,o}} = \frac{q_\alpha}{m_\alpha} \left( \frac{k^2}{\omega_\alpha^2 - \Omega_\alpha^2} \right) \tilde{\Phi} \quad (25)$$

$$\tilde{\mathbf{U}}_{\alpha,x} = \frac{q_\alpha}{m_\alpha} \left( \frac{k_x \omega_\alpha + i k_y \Omega_\alpha}{\omega_\alpha^2 - \Omega_\alpha^2} \right) \tilde{\Phi} \quad (26)$$

$$\tilde{\mathbf{U}}_{\alpha,y} = \frac{q_\alpha}{m_\alpha} \left( \frac{k_y \omega_\alpha - i k_x \Omega_\alpha}{\omega_\alpha^2 - \Omega_\alpha^2} \right) \tilde{\Phi} \quad (27)$$

With Eq. (25) and Eq. (6) the Guerrini<sup>10</sup> dispersion relation is found (see Eq. (28)). This dispersion relation is the starting point for understanding which instabilities are likely to contribute to transport, since it predicts the disturbances most likely to grow. Eq. (28) represents a 2-stream instability. In this case, the electrons are streaming with the classical drift velocity,  $|\mathbf{E}/\mathbf{B}|$ , in the azimuthal direction. The ions stream orthogonal to this. Since the system is not in equilibrium (with both species at the same average velocity), a parametric instability can occur.

$$1 = \frac{\omega_{p,e}^2}{\omega_e^2 - \Omega_e^2} + \frac{\omega_{p,i}^2}{\omega_i^2 - \Omega_i^2} \quad (28)$$

To understand if Eq. (28) predicts an instability, it must be solved for an arbitrary propagation direction for real  $k$  or real  $\omega$ . Here, the angle  $\theta$  is measured counterclockwise about  $\mathbf{B}$ , from the  $\mathbf{x}$  direction, and we solve for real frequency. For demonstration, Eq. (28) is solved for  $\mathbf{x} = -5\text{mm}$ , using experimental data collected by Hargus.<sup>5</sup> The result is shown in Fig. 2 and Fig. 3, as the solution to Eq. (28) with the highest spatial growth rate at a given propagation angle and frequency (if there is no growth rate, no solution is reported). Looking at Fig. 3, it is apparent that the propagation angle must be azimuthal, or somewhat azimuthal, for a convective instability to occur. If this is the case, instability is predicted for disturbances above  $\sim 1\text{MHz}$ . This is the primary reason that fluctuation-induced transport theories typically consider fluctuations that are azimuthal. In support of this approach, multi-MHz instabilities have been observed in the near-exit region of a Hall accelerator, and they appear to propagate in the azimuthal direction.<sup>11,12</sup>

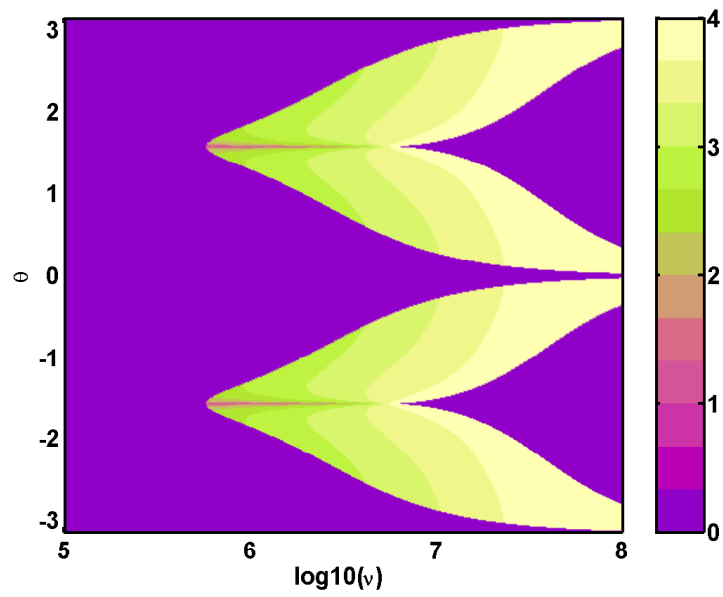


Figure 2.  $|\text{Re}(k)|$  for the solution with the highest growth rate at  $x = -5\text{mm}$ , in log scale.

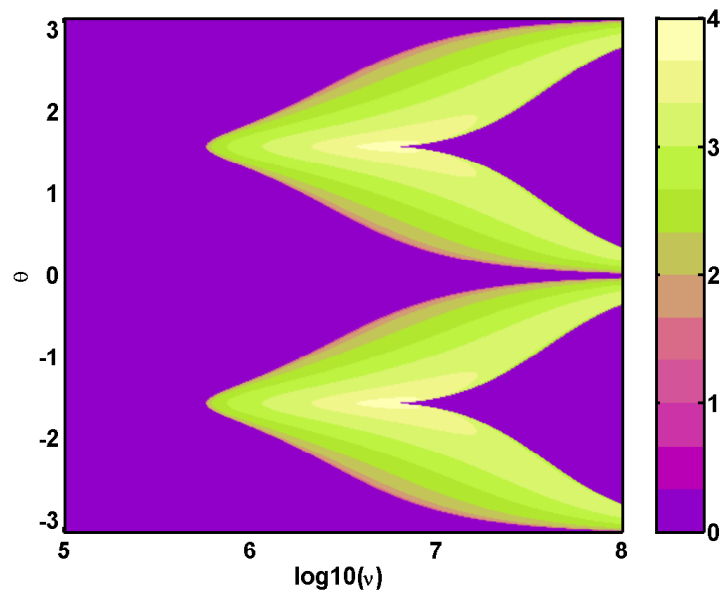


Figure 3.  $|\text{Im}(k)|$  for the solution with the highest growth rate at  $x = -5\text{mm}$ , in log scale.

## B. The Dispersion Relation (II)

In Sec. A, a dispersion relation is presented, Eq. (28), that estimates the frequency/wavenumber relationship of fluctuations in the Hall plasma accelerator. In deriving this expression several simplifications are used. These include the assumption that collisions and  $\mathbf{E} \times \mathbf{B}$  shear are negligible. In some regions of the HET this may be appropriate, but near the exit plane of the Stanford SPT, it is not. If these terms are included they alter the dispersion relation, and open new avenues for instability growth. In addition, they can cause a significant impact on anomalous transport.

If electron collisions and  $\mathbf{E} \times \mathbf{B}$  shear are included Eq. (28) becomes Eq. (29). All terms are unchanged in Eq. (28), except for a multiplier that operates on the electron fluid contribution to the dispersion relation.

$$1 = \left( \frac{\omega_{p,e}^2}{\omega_e^2 - \Omega_e^2} \right) \left( 1 + i\nu_e \omega_e^{-1} - i \cos \theta \sin \theta \frac{\partial \mathbf{U}_{e,o,y}}{\partial x} \omega_e^{-1} \right) + \frac{\omega_{p,i}^2}{\omega_i^2 - \Omega_i^2} \quad (29)$$

The added term may appear insignificant, but since it is often imaginary (and can be much greater than one), it can cause a substantial impact on magnitude of fluctuations, and their relative phase. This impacts anomalous transport. The solution to Eq. (29) is given in Fig. 4 and Fig. 5 at  $\mathbf{x} = -5\text{mm}$  in the Stanford SPT, including the electron-neutral collision rate, and the time-average  $\mathbf{E} \times \mathbf{B}$  shear. In these graphs, the solution with the greatest spatial growth-rate is provided as a function of propagation angle and real frequency. If there is no unstable solution nothing is reported. Fig. 4 and Fig. 5 display more structure than Fig. 2 and Fig. 3. This is a consequence of greater overall instability, and the occurrence of more unstable solutions. What is most interesting though, is the occurrence of unstable modes at non-azimuthal propagation angles. This is not predicted by Eq. (28) at  $\sim 1\text{MHz}$ , and could be important to transport physics. For reference, Fig. 6 and Fig. 7 provide the same solution as Fig. 4 and Fig. 5, over a smaller range of propagation angles.

Electron collisions and  $\mathbf{E} \times \mathbf{B}$  shear do more than alter spatial growth though, they also impact the phase relationship between fluctuations in the number density and fluctuations in the velocity. In Eq. (30) through Eq. (32), the relationship between fluctuations in the potential and fluctuations in the number density and velocity is reported.

$$\frac{\tilde{n}_\alpha}{n_{\alpha,o}} = \frac{q_\alpha}{m_\alpha} \left( \frac{k^2}{(\omega_\alpha + i\nu_\alpha)^2 - \Omega_\alpha^2} \right) \left( 1 + i\nu_\alpha \omega_\alpha^{-1} - i \cos \theta \sin \theta \frac{\partial \mathbf{U}_{\alpha,o,y}}{\partial x} \omega_\alpha^{-1} \right) \tilde{\Phi} \quad (30)$$

$$\tilde{\mathbf{U}}_{\alpha,x} = \frac{q_\alpha}{m_\alpha} \left( \frac{k_x(\omega_\alpha + i\nu_\alpha) + ik_y \Omega_\alpha}{(\omega_\alpha + i\nu_\alpha)^2 - \Omega_\alpha^2} \right) \tilde{\Phi} \quad (31)$$

$$\tilde{\mathbf{U}}_{\alpha,y} = \frac{q_\alpha}{m_\alpha} \left( \frac{k_y(\omega_\alpha + i\nu_\alpha) - ik_x \Omega_\alpha}{(\omega_\alpha + i\nu_\alpha)^2 - \Omega_\alpha^2} \right) \tilde{\Phi} \quad (32)$$

Here, it is assumed that the magnitude of the cyclotron frequency is much greater than the magnitude of the shear (in the Stanford SPT, the peak electron cyclotron frequency is an order of magnitude greater than the peak  $\mathbf{E} \times \mathbf{B}$  shear). Obviously, Eq. (31) and Eq. (32) are nearly identical to Eq. (26) and Eq. (27) (except for the collision term). The number density is impacted more. In Eq. (30), an extra term is added to the previous expression for the fluctuation in the number density (Eq. (25)). As a consequence, the phase of a number density fluctuation can be substantially altered when there is non-negligible shear, or a significant electron collision rate. As a consequence, electron collisions and/or shear can impact transport by changing which modes grow, and by altering the phase separating fluctuations in the number density and fluctuations in the velocity. In both cases, the *sign* of the shear is important.

Since Eq. (28) predicts azimuthal instabilities, but is rather simple, and even a small adjustment (representative of experimental findings) allows the prediction of axial and azimuthal instabilities, Eq. (29) is considered strong evidence that high-frequency azimuthal *and* axial instabilities likely occur in the near-exit region of the Hall-effect thruster. While several experiments have observed instabilities that appear azimuthal,<sup>13,14</sup> future experiments could encounter instabilities with a non-negligible axial component. In fact, experiments conducted with axially separated antenna may have observed axial disturbances at 2-5MHz<sup>15</sup> that were correlated to the discharge current. This is important, since results in Sec. III indicate that fluctuations with azimuthal and/or axial propagation vectors could be responsible for some portion of the anomalous transport in the near-exit region of the Hall accelerator.

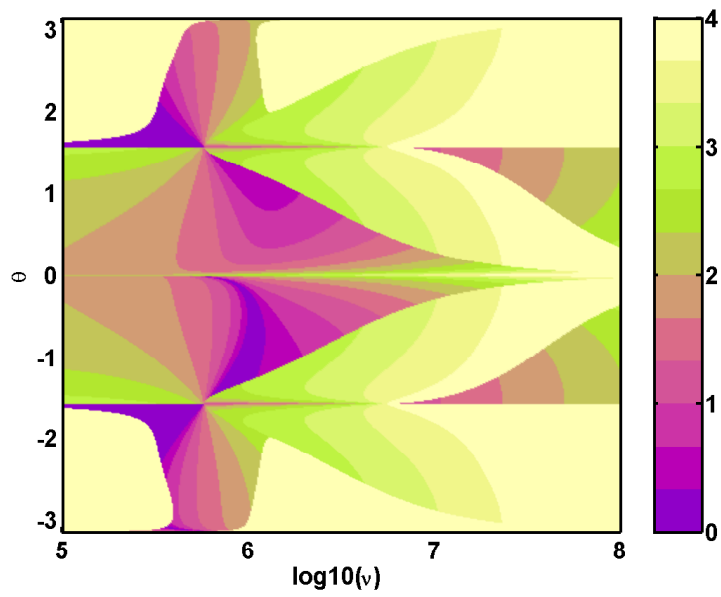


Figure 4.  $|\text{Re}(k)|$  for the mode with the highest growth rate at  $x = -5\text{mm}$ , in log scale.

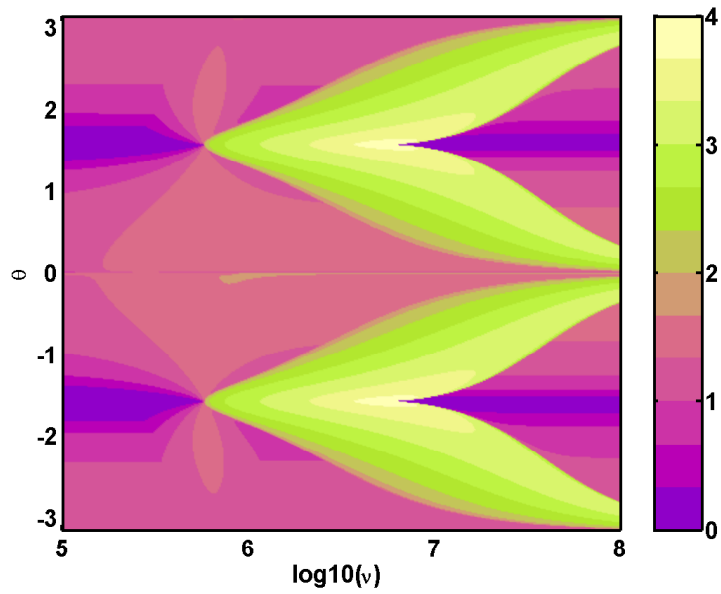


Figure 5.  $|\text{Im}(k)|$  for the mode with the highest growth rate at  $x = -5\text{mm}$ , in log scale.

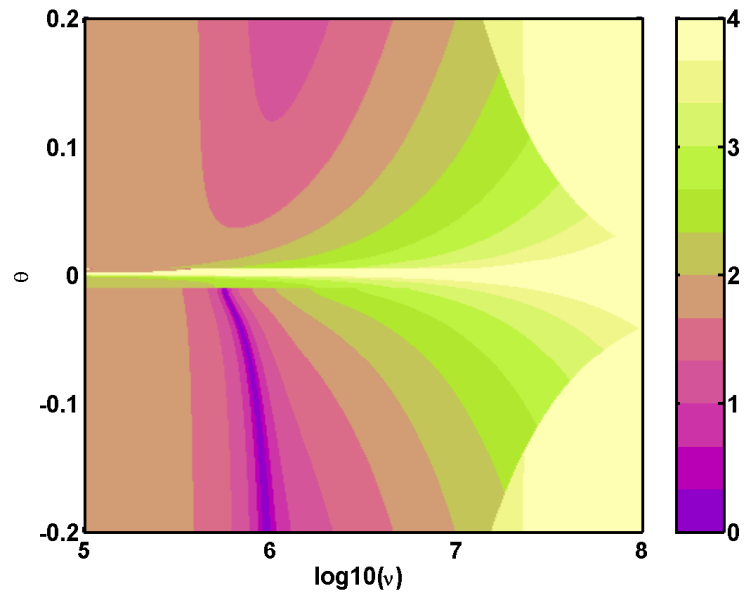


Figure 6.  $|\text{Re}(k)|$  for the mode with the highest growth rate at  $x = -5\text{mm}$ , in log scale.

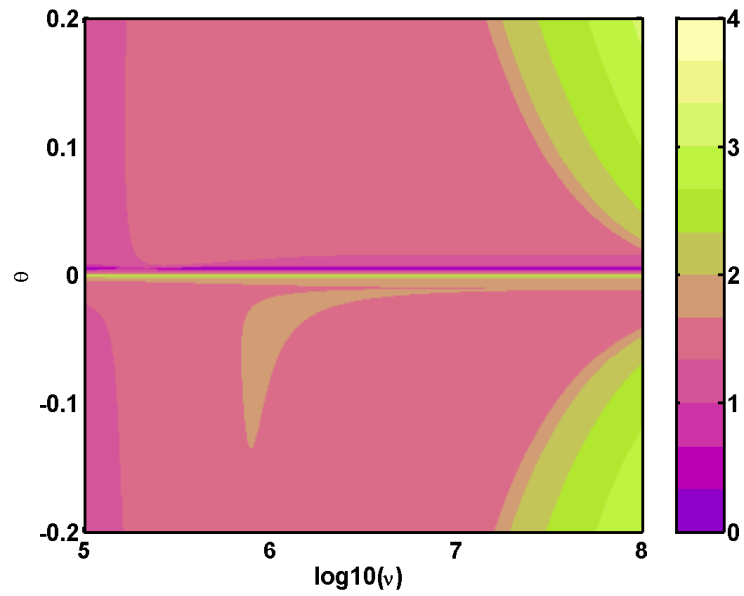


Figure 7.  $|\text{Im}(k)|$  for the mode with the highest growth rate at  $x = -5\text{mm}$ , in log scale.

### III. Fluctuation-induced Transport

The solution for small amplitude oscillations presented in Sec. II is readily applicable to a fluctuation-induced transport theorem, since for a given fluctuation in potential, the fluctuation in the number density and velocity is readily determined (see Eq. (25) through Eq. (27)). It should be stated of course, that for large amplitude fluctuations, Eq. (25) through Eq. (27) are only an approximation. Nevertheless, this equation set is a starting point for understanding anomalous transport due to plasma property fluctuations.

A quasi-linear model for the mobility is derived by considering the time-average current density. See Eq. (33).

$$\langle \mathbf{J}_\alpha \rangle = \langle q_\alpha n_\alpha \mathbf{U}_\alpha \rangle \quad (33)$$

As expected, a contribution to Eq. (33) comes from the time-average velocity,  $\mathbf{U}_{\alpha,o}$ , multiplied by the time-average number density,  $n_{\alpha,o}$ . This is termed the steady-state current (or base current) for species  $\alpha$  (see Eq. (34)).

$$\langle \mathbf{J}_\alpha \rangle_b = q_\alpha n_{\alpha,o} \mathbf{U}_{\alpha,o} \quad (34)$$

Less obvious, a time-average current can arise due to a fluctuating velocity and fluctuating number density due to their relative phase ( $\varphi$ ) - this happens even though the time-average value of a fluctuating quantity is zero. This current is ‘‘anomalous’’, since it is not predicted by a steady-state transport equation. See Eq. (35).

$$\langle \mathbf{J}_\alpha \rangle_a = \frac{1}{2} \mathbf{Re} \left( q_\alpha \tilde{n}_\alpha \tilde{\mathbf{U}}_\alpha^* \right) \quad (35)$$

This current is due to the fact that the velocity may be high when the number density is high (yielding a strong current in one direction), and the velocity may be low when the number density is low (yielding a weak current in the opposite direction). A time-average current can result.

Eq. (36) and Eq. (37) detail the anomalous current due to a disturbance that obeys Eq. (28). The total current is found by summing the base current and the anomalous current, and this is given by Eq. (38) and Eq. (39).

$$\langle J_{\alpha,x} \rangle_a = \left( \frac{q_\alpha n_{\alpha,o}}{2} \right) \left( \frac{q_\alpha}{m_\alpha} \right)^2 \mathbf{Re} \left( \left( \frac{k^2}{\Omega_\alpha^2 - \omega_\alpha^2} \right) \left( \frac{k_x \omega_\alpha + i k_y \Omega_\alpha}{\Omega_\alpha^2 - \omega_\alpha^2} \right)^* \right) \Phi \Phi^* \quad (36)$$

$$\langle J_{\alpha,y} \rangle_a = \left( \frac{q_\alpha n_{\alpha,o}}{2} \right) \left( \frac{q_\alpha}{m_\alpha} \right)^2 \mathbf{Re} \left( \left( \frac{k^2}{\Omega_\alpha^2 - \omega_\alpha^2} \right) \left( \frac{i k_y \omega_\alpha - k_x \Omega_\alpha}{\Omega_\alpha^2 - \omega_\alpha^2} \right)^* \right) \Phi \Phi^* \quad (37)$$

$$\langle J_{\alpha,x} \rangle = \langle J_{\alpha,x} \rangle_a + \langle J_{\alpha,x} \rangle_b \quad (38)$$

$$\langle J_{\alpha,y} \rangle = \langle J_{\alpha,y} \rangle_a + \langle J_{\alpha,y} \rangle_b \quad (39)$$

The solution to Eq. (38) and Eq. (39) is given for a 1eV fluctuation in the potential in Fig. 8, for the solution shown in Fig. 2 and Fig. 3. An inverse Hall Parameter  $\sim -1$  (in log scale) corresponds to Bohm-like transport, and so, transport comparable to Bohm is possible for reasonable choices of propagation angle and frequency (for a ‘‘small’’  $\tilde{\Phi}$ ). The classical inverse Hall parameter in this case is zero (no collisions). It is interesting to note, that for non-azimuthal propagation angles the transport is typically greater, though for a pure axial wave, the transport is almost classical. The propagation angle with the highest growth (see Fig. 3) is *not* the propagation angle with the greatest anomalous transport. Given that strong plasma property gradients in the axial direction are common in the Hall plasma accelerator, and that these gradients would likely refract pure-azimuthal plane waves, in combination with these findings, it is believed that the fluctuations responsible for anomalous transport in the HET are likely characterized by a non-zero axial wavenumber.

The solution to Eq. (38) and Eq. (39) for a 1eV fluctuation is interesting, but the choice of a 1eV fluctuation is arbitrary. In point of fact, this fluctuation in the potential can be considered large *or* small depending on the disturbance in question. Because of this, the magnitude of a fluctuation should only be judged in the context of the quasi-linear model (by considering the accuracy of the small amplitude

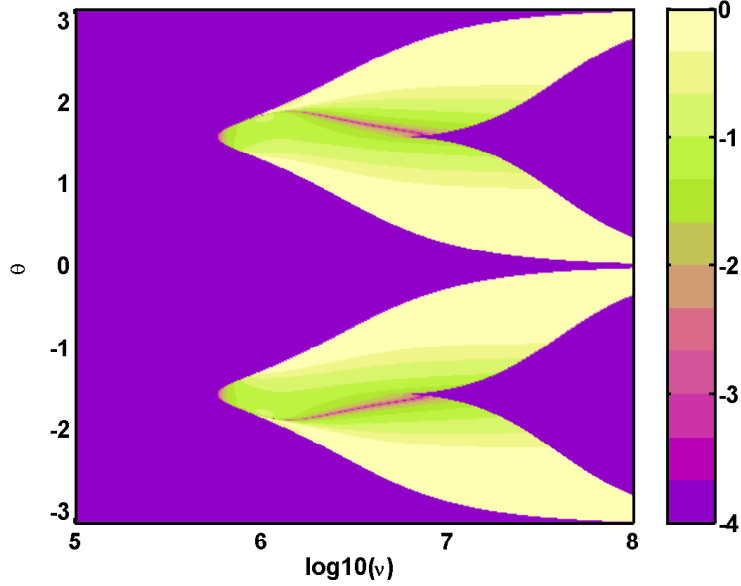


Figure 8.  $|(\omega\tau)^{-1}|$  in log scale, at  $x = -5\text{mm}$ , for a 1eV fluctuation.

approximation). A simple way to check (and find a reasonable limit on  $\tilde{\Phi}$ ), is to determine the potential fluctuation that will cause the small amplitude model to be inaccurate. For this purpose, we consider the species number density as a function of the potential, Eq. (25). If we dictate that the fluctuation in the number density must be less than its time-average value, a condition is found on the potential fluctuation for each species. See Eq. (40).

$$|\tilde{\Phi}| \ll \left| \frac{q_\alpha}{m_\alpha} \left( \frac{k^2}{\omega_\alpha^2 - \Omega_\alpha^2} \right) \right|^{-1} \quad (40)$$

As the magnitude of the left hand side of Eq. (40) approaches the magnitude of the right hand side, the small amplitude model becomes inaccurate. As a consequence, it is certain that Eq. (40) is not satisfied when both sides of Eq. (40) are equal. When the small amplitude model reaches this limit, the results of this section are inaccurate, and should not be extrapolated further. To this end, a limit is set for the potential (based on Eq. (40)), that dictates a “boundary” for the small amplitude model. See Eq. (41).

$$|\tilde{\Phi}|_{\max} = \frac{1}{4} \left| \frac{q_\alpha}{m_\alpha} \left( \frac{k^2}{\omega_\alpha^2 - \Omega_\alpha^2} \right) \right|^{-1} \quad (41)$$

The transport due to a potential fluctuation that satisfies Eq. 41 at  $x = -5\text{mm}$  is given by Fig. 9. Considering Fig. 9, it is observed that a 1eV fluctuation actually *exceeds* the small amplitude limit for most choices of frequency and propagation angle (since the inverse Hall Parameter in Fig. 9 is generally smaller than that in Fig. 8). Only for a limited range of primarily azimuthal propagation vectors, near the edge of instability onset, is the 1eV fluctuation small compared to Eq. 41. Regardless, the transport is much higher than classical in most circumstances. Given that experimental observations show an inverse Hall parameter of  $\sim 1/50$  at  $x = -5\text{mm}$ ,<sup>6</sup> it is apparent that coherent fluctuations may explain transport in the HET in the near-exit region. This conclusion is made even more certain, since more than one fluctuation may be present, and a more accurate account of non-linear effects could cause greater anomalous transport.

## IV. Summary

Through a careful treatment of each species’ mass and momentum conservation equations, and the electron energy conservation equation, this paper arrives at the dispersion relation for the Hall-effect thruster.

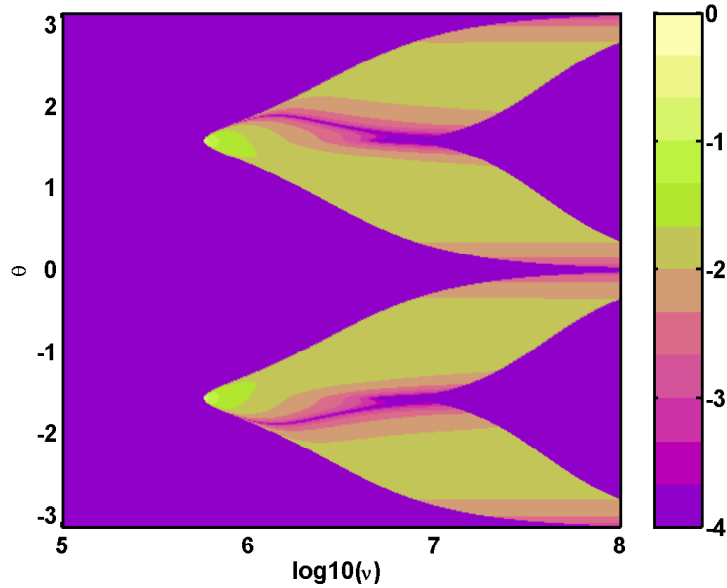


Figure 9.  $|(\omega\tau)^{-1}|$  in log scale, at  $x = -5\text{mm}$ , for a fluctuation that satisfies Eq. 41.

Depending on the terms included in the this relation, a variety of instabilities are found. Electron collisions, the electron temperature, and  $\mathbf{E} \times \mathbf{B}$  shear are found to impact the growth of instabilities, and in some cases, the phase separating  $\tilde{n}_\alpha$  and  $\tilde{\mathbf{U}}_\alpha$ . To determine whether the observed instabilities could explain anomalous transport, the current induced by  $\tilde{n}_\alpha$  and  $\tilde{\mathbf{U}}_\alpha$  is calculated for small-amplitude fluctuations. Using this model, significant transport is predicted for disturbances in certain frequency/wavenumber regimes. Bohm-like transport is found under certain circumstances. As a consequence, it is concluded that transport in the Hall-effect thruster could result from small-amplitude fluctuations, and that spatial dependence in the time-average mobility could result from a position dependent oscillation spectra.

Future research will consider which modes dominate anomalous transport in the Hall-effect thruster, and examine the origin of and saturation of various disturbances (in the axial-azimuthal plane). It is believed that the fluctuations important to transport at a given location may not be determined by local stability criteria. Instead, a global model may be needed to predict the oscillation spectra at a given location. Also, the appropriateness of the small amplitude model will be considered, and the impact of large amplitude fluctuations will be calculated. It is thought that significant anomalous transport is likely in a regime where nonlinear effects become important, and that fluctuation-induced transport in the HET may be better described by large-amplitude oscillations.

## Acknowledgements

Funding for this research was provided by the Air Force Office of Scientific Research. C. Thomas received support from the National Science Foundation, and also from Stanford University, through the Stanford University Graduate Fellowship Program.

## References

- <sup>1</sup>Zhurin, V., Kaufman, H., and Robinson, R., "Physics of closed drift thrusters," *Plasma Sources Science and Technology*, Vol. 8, No. R1, 1999.
- <sup>2</sup>Hagelaar, G., Bareilles, J., Garrigues, L., and Boeuf, J., "Role of anomalous electron transport in a stationary plasma thruster simulation," *Journal of Applied Physics*, Vol. 93, No. 67, 2003.
- <sup>3</sup>Fife, J., *Hybrid-PIC Modeling and Electrostatic Probe Survey of Hall Thrusters*, Ph.D. thesis, Massachusetts Institute of Technology, 1998.
- <sup>4</sup>Bishaev, A. and Kim, V., "Local plasma properties in a Hall-current accelerator with an extended acceleration zone,"

*Sov. Phys. Tech. Phys.*, Vol. 23, No. 9, 1978.

<sup>5</sup>Hargus, W., *Investigation of the Plasma Acceleration Mechanism within a Coaxial Hall Thruster*, Ph.D. thesis, Stanford University, 2001.

<sup>6</sup>Meezan, N., Hargus, W., and Cappelli, M., "Anomalous electron mobility in a coaxial Hall discharge plasma," *Physical Review E*, Vol. 63, No. 026420, 2001.

<sup>7</sup>Bohm, D., Burhop, E., and Massey, H., *The Characteristics of Electrical Discharge in Magnetic Fields*, McGraw Hall, 1949.

<sup>8</sup>Meezan, N. and Cappelli, M., "Kinetic study of wall collisions in a coaxial Hall discharge," *Physical Review E*, Vol. 66, No. 036401, 2002.

<sup>9</sup>Barral, S., Makowski, K., Peradzynski, Z., Gascon, N., and Dudeck, M., "Wall material effects in stationary plasma thrusters. II. Near-wall and in-wall conductivity," *Physics of Plasmas*, Vol. 10, No. 10, 2003.

<sup>10</sup>Guerrini, G. and Michaut, C., "Characterization of high frequency oscillations in a small Hall-type thruster," *Physics of Plasmas*, Vol. 6, No. 1, January 1999, pp. 343–349.

<sup>11</sup>Litvak, A., Raitses, Y., and Fisch, N., "Experimental studies of high-frequency azimuthal waves in Hall thrusters," *Physics of Plasmas*, Vol. 11, No. 4, April 2004, pp. 1701–1705.

<sup>12</sup>Lazurenko, A., Vial, V., Prioul, M., and Bouchoule, A., "Experimental investigation of high-frequency drifting perturbations in Hall thrusters," *Physics of Plasmas*, Vol. 12, No. 013501, November 2005, pp. 1–9.

<sup>13</sup>Smirnov, A., Raitses, Y., and Fisch, N., "Electron Transport and Ion Acceleration in a Low-Power Cylindrical Hall Thruster," *40th AIAA/ASME/SAE/ASEE Joint Propulsion Conference and Exhibit*, No. AIAA-2004-4103.

<sup>14</sup>Cedolin, R., *Laser-induced fluorescence diagnostics of xenon plasmas*, Ph.D. thesis, Stanford University, 1997.

<sup>15</sup>Thomas, C., Gascon, N., and Cappelli, M., "Spatial and Temporal Mapping of Azimuthal Current in a Hall Thruster," *39th AIAA/ASME/SAE/ASEE Joint Propulsion Conference and Exhibit*, No. AIAA-2003-4854.